Statistical Properties of Electron Curtain Precipitation Estimated with AeroCube-6

M. Shumko[1,2], A.T. Johnson[1], T.P. O'Brien[3], D.L. Turner[4], A.D. Greeley[2], J.G. Sample[1], J.B. Blake[3], L.W. Blum[2], A.J. Halford[2]

[1]Department of Physics, Montana State University, Bozeman, Montana, USA
[2]NASA's Goddard Space Flight Center, Greenbelt, Maryland, USA
[3]Space Science Applications Laboratory, The Aerospace Corportation, El Segundo, California USA
[4]Johns Hopkins Applied Physics Laboratory, Laurel, Maryland, USA

Key Points:

- We used the dual AeroCube-6 CubeSats to identify stationary, narrow in latitude, and persistent > 30 keV precipitation in low Earth orbit
- 90% of curtains observed are narrower than 21 kilometers in latitude
- A few curtains persistently scattered into the atmosphere for at least six seconds

Corresponding author: M. Shumko, `msshumko@gmail.com`

Abstract

Curtains are a stationary, persistent, and narrow in latitude electron precipitation phenomenon recently discovered in low Earth orbit over sequential passes of the dual AeroCube-6 CubeSats. Curtains with $>$ 30 keV electron energies were stationary over a variety of spacecraft separations, and observed by the follower spacecraft for up to 65 seconds after the leader. This study expands on the recent curtain discovery and quantifies statistical properties of 1634 curtains observed over three years. We found that in low Earth orbit, many curtains are narrower than 10 kilometers in latitude and 90% are narrower than 21 kilometers. We also found that curtains are an outer radiation belt phenomena that are observed in the late morning and midnight magnetic local time, with a higher occurrence rate at midnight. Furthermore, curtains are observed more often during geomagnetically active times. We compared these statistical results to microbursts and tested the hypothesis that curtains are drifting remnants of microbursts. Lastly, we found a few curtains in the bounce loss cone region in the north Atlantic Ocean where particle drift motion is impossible. One of these curtains continuously scattered for at least six seconds, therefore curtains can be a significant source of $>$ 30 keV electrons into the atmosphere.

1 Plain Language Summary

Electron curtain precipitation is a recently-discovered phenomenon observed by dual-spacecraft missions such as the AeroCube-6 CubeSats that orbit 700 kilometers above Earth's surface. Curtains appear stationary, remaining unchanged from seconds to a minute. Curtains are also very narrow along the satellite orbit (mostly in latitude). Besides these two properties, curtains and their impact on the magnetosphere and atmosphere are not well understood. This study found 1634 curtains observed by the AeroCube-6 mission over a three year period and quantified their properties to better understand their origin. Curtains are hypothesized to be related to another form of electron precipitation called microbursts and we tested this hypothesis. This study found that curtains and microbursts share many similarities, however curtains observed in a special region in the North Atlantic Ocean put this hypothesis in question. A few dozen curtains observed in this North Atlantic region were precipitating into the atmosphere for multiple seconds and are unlikely to be related to microbursts. Therefore, curtains may be a significant source atmospheric ionization responsible for the natural degregation of ozone.

2 Introduction

Curtain electron precipitation is a stationary phenomenon observed in low Earth orbit (LEO). Curtains are narrow in latitude and appear stationary for up to a minute between subsequent satellite passes. Consider rewording: Blake and O'Brien (2016) recently discovered curtains with the $>$ 30 keV electron dosimeters onboard the dual AeroCube-6 (AC6) CubeSats that operated together between 2014 and 2017. This discovery was possible due to AC6's actively maintained in-track separation that varied between a few hundred meters and a few hundred kilometers. Besides the Blake and O'Brien (2016) discovery study not much is known about curtains including, what they are, how are they generated, their statistical properties, and their impact on the atmosphere. Answering these questions is an essential next step towards a more complete understanding of how curtains, and particle precipitation in general, affect the magnetosphere and Earth.

In low Earth orbit curtains are narrower than a few tens of kilometers in latitude so a polar-orbiting LEO satellite, such as AC6, will pass through their cross-section in about a second. Curtains appear sharply peaked in the electron data. AC6 also observes similar-looking transient precipitation called electron microbursts. Both microbursts and curtains are peaked in the AC6 data for different reasons: microbursts primarily for being temporally short, and curtains primarily for being narrow in latitude. Hence AC6,

and other recently developed multi-spacecraft missions, are necessary to identify and distinguish between curtains and microbursts.

Since the mid 1960s, microbursts have been observed by high altitude balloons where they also appear as sharp peaks with a sub-second duration (e.g. Anderson & Milton, 1964; Brown et al., 1965; Parks, 1967). Because balloons are relatively stationary, a microburst is easy classified as a transient phenomenon. Microburst electrons have also been directly observed by LEO satellites (e.g. Lorentzen, Blake, et al., 2001; O'Brien et al., 2003; Douma et al., 2017). But precipitation that looks like a microburst from a single LEO satellite is ambiguous—it can be either transient or stationary. Thus, multi-spacecraft missions such as the Focused Investigations of Relativistic Electron Burst Intensity, Range, and Dynamics (Johnson et al., 2020, FIREBIRD-II) and AC6 (O'Brien et al., 2016) are necessary to resolve this ambiguity. The companion study to this work used the AC6 CubeSats to find transient microbursts that were observed simultaneously by both spacecraft to estimate the spatial size of microbursts (Shumko et al., 2019).

The impact of microbursts on the environment is substantial. Lorentzen, Looper, and Blake (2001), Thorne et al. (2005), Breneman et al. (2017), and Douma et al. (2019)—among others—estimated that microbursts can deplete the outer radiation belt electrons in about a day. Furthermore, Seppälä et al. (2018) modeled a 6 hour microburst storm and concluded that microbursts depleted mesospheric ozone by roughly 10%. Thus, it is important to understand the connection, if any, between microbursts and curtains. Curtains and microbursts can be easily misidentified from a single spacecraft so we need to reevaluate single-satellite microburst studies. If curtains are numerous then the estimated microburst occurrence rates are overestimated. Furthermore, the microburst impact on the atmosphere and the outer radiation belt is overestimated.

Blake and O'Brien (2016) proposed the following hypothesis that explains the curtain-microburst relationship. If a microburst is not completely lost in the atmosphere after the initial scatter, the remaining microburst electrons will spread out (bounce phase disperse) along the entire magnetic field line over a few bounce periods. Concurrently these electrons drift to the east, with higher energy electrons drifting at a faster rate. Therefore, if this hypothesis is true, the initially localized microburst is spread out in longitude into the shape of a curtain. The idea of curtains is not entirely new, and Lehtinen et al. (2000) presented a different hypothesis that curtains can be created by energetic runaway beams driven by lightning.

This study expands the Blake and O'Brien (2016) study by estimating statistical properties of curtains. We use 1634 confirmed curtain observations to study the distributions of: the curtain width in latitude, the geomagnetic conditions favorable to curtains, and curtain distribution in L and magnetic local time (MLT). Lastly we will address the hypothesis that curtains are drifting remnants of microbursts by showing examples of curtains observed in the BLC region.

3 Instrumentation

The AC6 mission was a pair of 0.5U (10x10x5 cm) CubeSats built by The Aerospace Corporation and designed to measure the electron and proton environment in low Earth orbit (O'Brien et al., 2016). AC6 was launched on 19 June 2014 into a 620x700 km, 98° inclination orbit. The AC6 orbit over the three year mission lifetime was roughly dawn-dusk, and precessed only a few hours in MLT; 8-12 MLT in dawn and 20-24 MLT in dusk. The two AC6 spacecraft, designated as AC6-A and AC6-B, separated after launch and were in proximity for the duration of the three-year mission—maintained by an active attitude control system. The attitude control system allowed them to precisely control the amount of atmospheric drag experienced by each AC6 unit using the surface area of their solar panel "wings". By changing their orientation, AC6 was able to maintain

a separation between 2-800 km, confirmed with the Global Positioning System. The two AC6 units were in a string of pearls configuration so one unit, typically unit A, was leading the other by an in-track lag—the time it would take the following spacecraft to catch up to the position of the leading spacecraft. To convert between the AC6 in-track separation and in-track lag, we use a typical 7.5 km/s LEO velocity. The in-track lag was readily available with the Global Positioning System which makes it easy to study precipitation phenomena observed at the same time, and at the same position by shifting one time series by the in-track lag.

Each AC6 unit contains three Aerospace microdosimeters (licensed to Teledyne Microelectronics, Inc) that measure the electron and proton dose in orbit (O'Brien et al., 2016). The dosimeter used for this study is dos1 with a 30 keV electron threshold. dos1 is used for this study because the other dosimeters either responded primarily to protons or were not identical between unit A and B. All dosimeters sample at 1 Hz in survey mode, and 10 Hz in burst mode. 10 Hz data was readily available from both AC6 units from June 2014 to May 2017 while their in-track lag was less than 65 seconds, and at times was a fraction of a second. Figure A1 shows the distribution of 10 Hz data as a function of AC6 in-track lag. The variety of AC6 separations and data availability over the three-year mission makes it possible to study tranisent electron microburst precipitation (Shumko et al., 2019) and now stationary electron curtain precipitation.

4 Methodology

4.1 Curtain Identification

The 10 Hz data was used to identify curtains with the following two criteria that are described below: a high spatial correlation, and peaked. Before we applied the identification criteria, the AC6-B time series was shifted by the in-track lag to spatially align it with the AC6-A time series.

The first identification criterion is a 1-second rolling Pearson correlation applied to both time series. Spatial features with a correlation greater than 0.8 are considered highly correlated. The second criterion is applied to any features determined to be highly correlated to check if they are also peaked. Similar to how precipitation bands were identified by Blum et al. (2015) and microbursts by Greeley et al. (2019), we find peaked precipitation by quantifying the number of Poisson standard deviations, σ, that a dos1 count rate is above a 10-second centered running average, B_{10}. Locations where dos1 is at least two σ above B_{10}, in other words $dos1 > 2\sqrt{B_{10}} + B_{10}$, are considered peaked.

We tuned the detection parameters to identify many candidate curtains while being feasible to check every detection. One author visually inspected 6149 candidate curtains and 1634 quality curtains were confirmed. Four curtain examples are shown in Fig. 1. In each example, the unmodified time series is shown in the top row and the spatially-aligned time series the bottom row. The in-track lag used to shift the bottom row is annotated by dt, corresponding to an AC6 in-track separation annotated by s. The bottom row shows highly correlated curtains observed at the same location for at least 3 to 26 seconds.

4.2 Differentiating Between Drifting and Precipitating Curtains

The AC6 dosimeters lack the necessary pitch angle resolution to differentiate between drifting and precipitating electrons to test the Blake and O'Brien (2016) hypothesis. One common method of distinguishing between precipitating, drifting, and trapped particles is using particle measurements in conjunction with the location of the South Atlantic Anomaly (SAA).

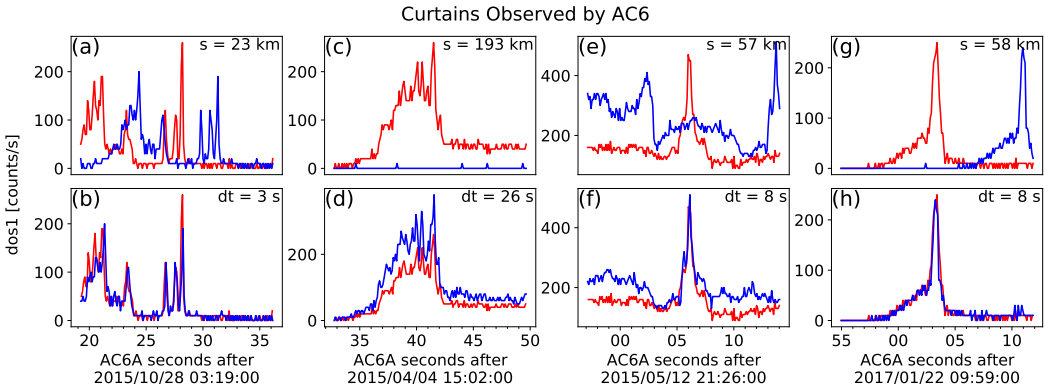

Figure 1. Four examples showing the AC6 $>$ 30 keV electron data taken by AC6 at the same time in the top row and at the same position in the bottom row. AC6-A, whose data is shown with red curves, was s kilometers ahead of AC6-B. To show the data at the same position the AC6-B time series was shifted by the in-track lag annotated by dt. These examples show that curtain precipitation was highly correlated for up to 26 seconds.

Earth's magnetic field is asymmetric which creates a region of weaker magnetic field in the South Atlantic Ocean called the South Atlantic Anomaly. While some particles observed in LEO are trapped and will execute closed drift paths, most particles observed in LEO are quasi-trapped: they drift around the Earth until they reach the SAA. Within the SAA, the weaker magnetic field strength can lower the electron's mirror point altitude into the atmosphere, where collisions with the atmospheric ions are more numerous and the particle is lost.

Particles that have pitch angles in the drift loss cone will precipitate within one drift period (often within the SAA). Particles with smaller equatorial pitch angles (less than about 10°) that are lost in the atmosphere within one bounce are in the bounce loss cone (BLC). Traditionally, we define a particle to be in the BLC if its mirror point altitude is at or below 100 km in either hemisphere.

In most regions outside of the SAA and its conjugate point in the North Atlantic, AC6 will observe electrons in both the drift and bounce loss cones. In the SAA, AC6 does not only observe electrons that are immediately lost, but a combination of electrons that are in the drift loss cone, bounce loss cone, and trapped (a trapped electron that locally mirrors at AC6's altitude in SAA will mirror higher everywhere else). In the region magnetically conjugate to the SAA in the North Atlantic, AC6 only observes electrons in the BLC. Here, if an electron makes it to AC6's altitude, it might be in the local loss cone and precipitate in the local hemisphere. Alternatively, the electron will mirror at or below AC6 and bounce to the conjugate mirror point in the SAA where the mirror point is deep in the atmosphere or below sea level. Therefore, any precipitation observed in this region must rapidly precipitate.

We estimated the BLC region for locally-mirroring electrons in the North Atlantic Ocean using the IRBEM-Lib magnetic field library and the Olson-Pfitzer magnetic field model (Boscher et al., 2012; Olson & Pfitzer, 1982). We defined a latitude-longitude grid spanning the North Atlantic at 700 kilometer altitude (a typical altitude for AC6), and estimated the local magnetic field strength. For each latitude-longitude point we traced the magnetic field line to the southern hemisphere and found the conjugate mirror point altitude. If the conjugate mirror point is at or below 100 kilometers, the electron is likely lost and the assosiated grid point is considered to be in the BLC. Furthermore, a more rigorous bounce loss cone criterion would be if the conjugate mirror point altitude is be-

low sea level. In this case, the electron is definitely lost. Since AC6 can measure locally-mirroring electrons in the North Atlantic, the spacecraft altitude determines the upper bound conjugate mirror point altitude in the SAA. The BLC region estimated by this method closely matches the BLC region shown in Comess et al. (2013, Figure 1) and Dietrich et al. (2010, Figure 3). Furthermore, we repeated the same analysis using the Tsyganenko 1989 model (Tsyganenko, 1989), which yielded similar boundaries.

5 Results

In the spirit of brevity, we limited the scope of this statistical study to answer three questions:

1. What is the distribution of curtain widths in latitude?
2. When and where are curtains observed?
3. Are curtains drifting or locally precipitating?

We will then compare some of these results to the > 30 keV microburst distribution from Shumko et al. (2019).

5.1 Curtain Width

We quantified curtain width in the time series as the width at half of the curtain's topographic prominence: the height of the peak above the lowest contour that encircles the peak but contains no higher peak. The spatial width of a curtain is then the product of the observed width in time and the 7.5 km/s orbital velocity. The curtain width is measured along AC6's orbit track that is mostly in latitude, therefore the estimated curtain widths are also approximately in latitude. The distribution of curtain widths is shown in Fig. 2 by the thick black curve. Curtains are very narrow. Many curtains are less than 10 km wide, and 90% are narrower than 21 km in latitude.

We compared the curtain width distribution to the microburst size distribution estimated in Shumko et al. (2019). Shumko et al. (2019) estimated the microburst size distribution by finding microbursts that were observed simultaneously by both AC6 units so the microburst size must be larger than the AC6 separation. The red curve in Fig. 2 shows the microburst distribution estimated by the ratio of the number of concurrent and nonconcurrent microbursts observed in each separation bin.

5.2 When and Where Are Curtains Observed

The distribution of curtains in L and MLT is shown in Fig. 3. Figure 3a shows the distribution of the observed curtains while Fig. 3b shows the same distribution normalized by the number of quality 10 Hz samples AC6 took at the same location in each L-MLT bin. This normalization is shown in Fig. 3c. The white bins in the early morning and evening MLT regions in Fig. 3a had no observed curtains because AC6 did not orbit there as confirmed by Fig. 3c. The normalized curtain distribution in Fig. 3b shows an enhanced curtain occurrence in the outer radiation belt in late morning and midnight MLT regions.

Now we quantify the geomagnetic conditions favorable for curtains. Figure 4 shows the distribution of the Auroral Electroject (AE) index between 2014 and 2017 in solid black. The distribution of the AE index when curtains were observed is shown by the dotted blue lines. Lastly, the distribution of the AE index when > 30 keV microbursts were observed is shown with a dashed green lines. Both microbursts and curtains are observed during active geomagnetic times. Is the normalized version of Fig. 4 insightful?

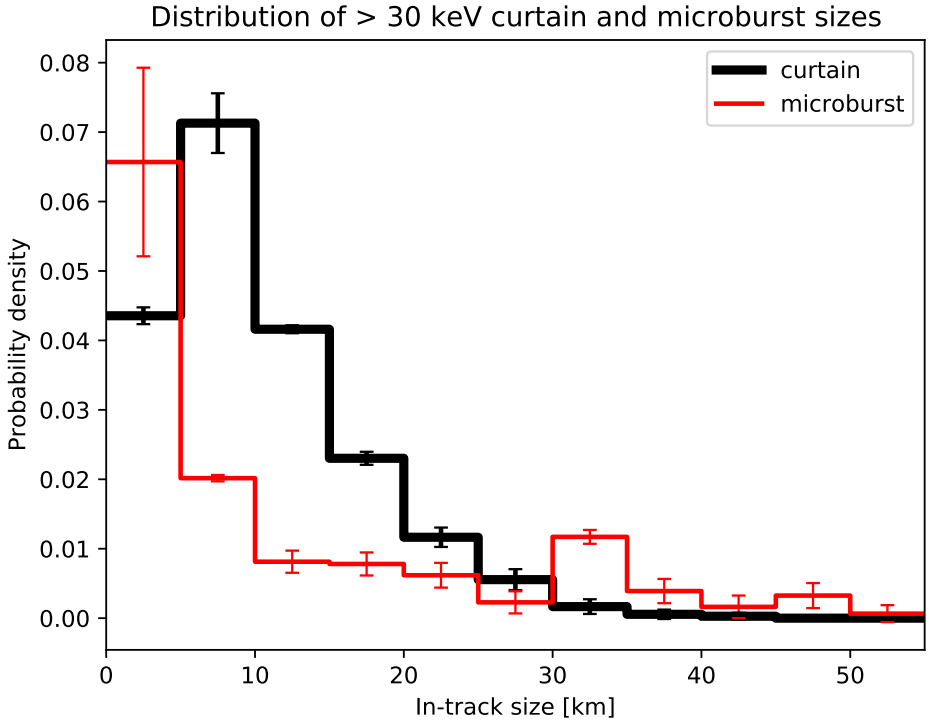

Figure 2. The distribution of curtain width in latitude is shown by the thick black lines. Furthermore, distribution of microburst sizes is shown by the red lines for microbursts that were simultaneously observed by AC6. The microburst distribution is adapted from Shumko et al. (2019). The error bars represent the Poisson standard error.

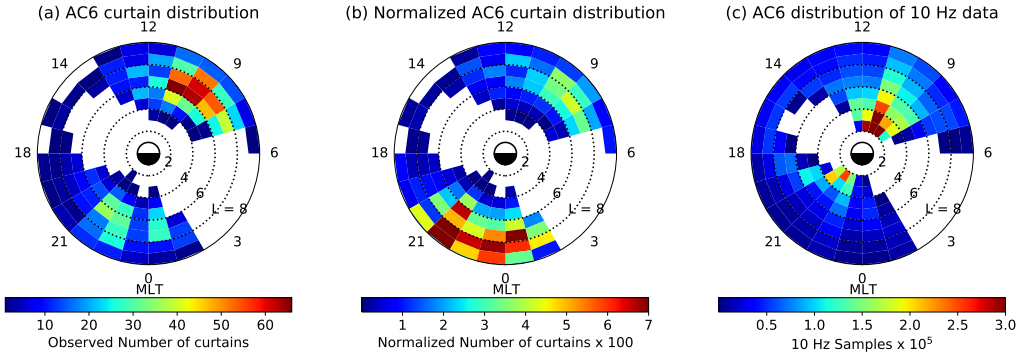

Figure 3. The distribution of observed curtains by L shell and MLT. Panel a shows the locations of all observed curtains used in this study. Panel b shows the curtain distribution normalized by the number of quality 10 Hz samples taken in each bin, shown in panel c. The white bins in panels a and b show where no curtains were observed. In panel c the white bins show where AC6 did not take any 10 Hz data together.

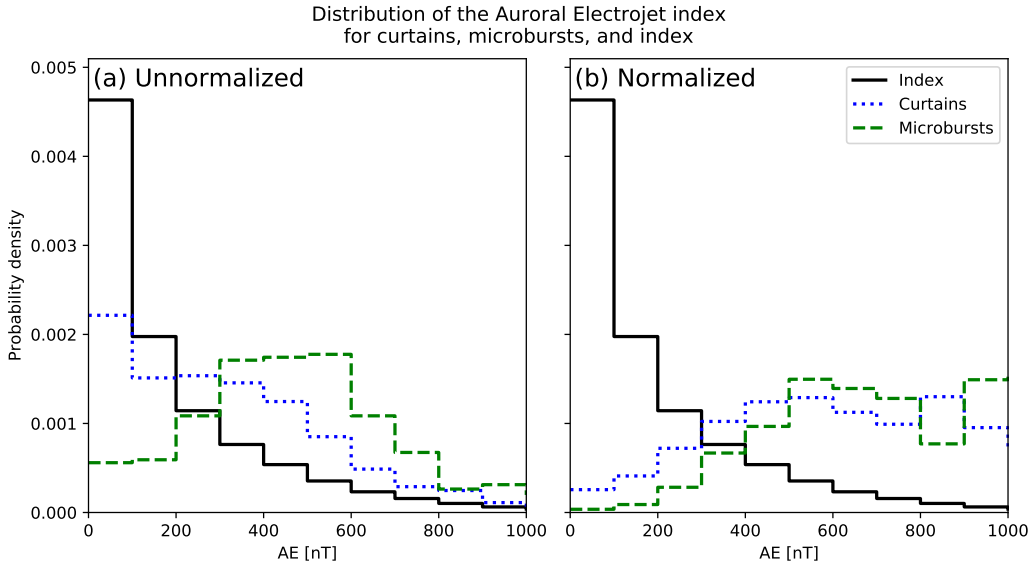

Figure 4. The distribution of the Auroral Electroject (AE) index from 2014 to 2017. The black curve shows the distribution for the AE index between 2014 and 2017. In panel a the dotted blue curve shows the AE distribution for curtains, and the dashed green curve shows the AE distribution for microbursts studied in Shumko et al. (2019). Panel b shows the same distribution of the AE index, and the normalized curtain and microburst distributions, normalized by the AE index. Show the normalized version of this plot?

5.3 Local Atmospheric Precipitation

Figure 5a shows a map of the northern BLC region in the North Atlantic. The solid blue line is the northern boundary where an electron that mirrors locally at 700 km has a conjugate mirror point at 100 km in the SAA. Immediately south of the solid blue line, the conjugate mirror altitude rapidly decreases towards, and below, sea level. The dashed blue line is the boundary where the conjugate mirror point altitude is at sea level. South of this line the mirror point is inside Earth. For reference, AC6 takes about 30 seconds to move between the solid and dashed blue curves. The two dotted black curves in Fig. 5a are roughly the boundary of the outer radiation belt, defined as $L = 4 - 8$.

We found 36 curtains that were observed inside the BLC region. Figure 5b-e shows 4 curtain examples (AC6-B time shifted by the in-track lag), along with the AC6 in-track lag, L and MLT during the observations annotated. The AC6 locations where these curtains were observed are shown in Fig. 5a with red stars and the corresponding panel labels.

6 Discussion

6.1 Curtain Width

Curtains are very narrow along the AC6 orbit track which is mostly in latitude. Figure 2 shows that the width of most curtains is on the order of 10 kilometers and 90% are narrower than 21 km. Scaled to the magnetic equator, where we presume curtains are generated, these widths correspond to a source with a radial scale size of a few hundred kilometers. As shown in Fig. 1, it is remarkable that some curtains remain stationary and maintain a fine structure after multiple seconds with little observable difference.

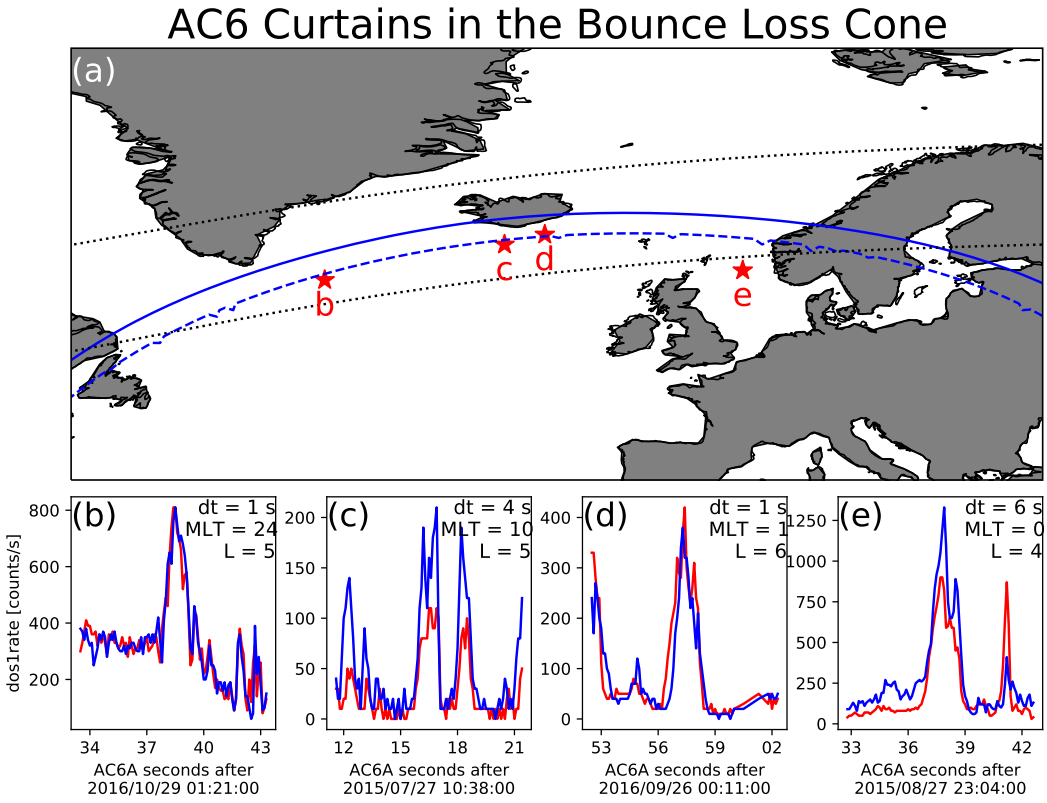

Figure 5. Curtains observed in the bounce loss cone region. Panel a shows a map of the North Atlantic region with the outer radiation belt, defined by $L = 4 - 8$, shown with the dotted black curves. The solid blue curve shows the northern boundary of the bounce loss cone region. Along this curve, electrons locally mirroring at 700 kilometers altitude in the North Atlantic have a conjugate mirror point at 100 kilometers altitude in the SAA. A more strict bounce loss cone criterion is the dashed blue curve that represents a mirror point altitude at sea level in the SAA. The 4 red stars with labels show the locations of the curtain examples shown in panels b-e. The panels b-e show the 4 example curtains with the AC6-A data shown by the red line and the time-shifted AC6-B data with the blue line. AC6-A was ahead in all examples except panel d.

However, some curtains appear to be slightly and systematically shifted in latitude, while maintaining their fine structure (not shown).

If curtains are remnants of microbursts then the distribution of curtain widths in latitude correspond to the microburst size distribution. Figure 2 shows a good correspondence between the distribution of curtain widths in latitude and the microburst size distribution from Shumko et al. (2019). Therefore, it is reasonable to believe that curtains and microbursts are related, but this result needs to be closely inspected for sources of bias.

The microburst scale size distribution, as described in Shumko et al. (2019), is the fraction of microbursts observed simultaneously to all microbursts observed either simultaneously or by only one AC6 unit. A microburst observed simultaneously must be larger than the spacecraft separation so the microburst distribution is a lower bound. Furthermore, the detection algorithm described in section 4.1 loses sensitivity for wider curtains. For curtains with a width similar to the detection algorithms 10-second baseline, the baseline will be artificially elevated making the curtain peak less pronounced. The result of this bias is similar to the bias inherent in the microburst distribution—both distributions are underestimated. These biases are difficult to quantify but we believe that they do not qualitatively change the interpretation of Fig. 2 that microburst and curtain size distributions are similar.

6.2 When and Where Are Curtains Observed

Figure 3b shows that curtains originate in the outer radiation belt and is observed relatively more in the late evening than late morning regions. Unfortunately, the limited AC6 coverage prevents a complete curtain distribution in MLT. This distribution, though limited, appears to be similar to the L-MLT distribution of microbursts from prior studies (e.g. O'Brien et al., 2003; Douma et al., 2017). The MLT region with the most frequently observed curtains and microbursts are opposite: microbursts are preferentially observed in the late morning, while curtains are mainly observed near midnight. The statistics at high L are rather limited because AC6 rapidly crosses high L shells, nevertheless Fig. 3b hints that curtains near midnight MLT were observed to L shells possibly farther out than the outer radiation belt.

Figure 4 shows that the microburst and curtain observations are both associated with an enhanced AE. The occurrence rate of microbursts increases with enhanced AE more than the occurrence rate of curtains. Are the following sentences still relevant with the normalized distribution? One possible explanation is that during quiet conditions the remnant microburst electrons are more likely to drift undisturbed and AC6 is more likely to observe the fine, highly-correlated curtain structure. In contrast, during active conditions curtain electrons are still drifting, but the dynamics of an actively-changing magnetosphere can easily perturb curtain electrons until AC6 no longer observes a highly correlated structure at the same location.

6.3 Curtains Observed in The Bounce Loss Cone

The evidence presented so far hint at, but not directly confirm that, curtains are connected to microbursts. But the few curtains that were observed in the bounce loss cone and shown in Fig. 5 put the hypothesis into question. These curtains were observed near the sea level mirror altitude curve thus they were not drifting and were precipitating for as long as 6 seconds as shown in Fig. 5e. The curtain precipitation persisted for multiple bounce periods (≈ 1.5 seconds for 30 keV electrons in this region). What can cause continuous > 30 keV electron precipitation lasting for multiple seconds? This mechanism must be radially localized near the magnetic equator, on a scale of a few hundred kilometers. A candidate mechanism is a direct current electric field that is parallel to

the background magnetic field that lowers the electron mirror point to AC6 altitudes. To find the minimum potential we assume the electron is barely trapped and has a 100 kilometer conjugate mirror point altitude in the SAA, so initially the electron will mirror above AC6 in the bounce loss cone region.

To find the parallel potential, $q\Phi$, we use the kinetic energy, W, of a 30 keV electron at its initial mirror point with a magnetic field strength of B_i. The kinetic energy at the initial mirror point can be written as $W_i = \mu B_i$ where μ is the first adiabatic invariant that is conserved during this acceleration. When a parallel potential acts on the electron of charge q and does $q\Phi$ amount of work the electron will mirror closer to Earth's surface and mirror at a field strength B_f where its final energy is $W_f = \mu B_f$. Now we relate the initial and final kinetic energy of the electron,

$$\mu B_f = \mu B_i + q\Phi. \tag{1}$$

Then we solve for $q\Phi$ and substitute μ to express the above equation as a function of the initial kinetic energy

$$q\Phi = W_i \frac{(B_f - B_i)}{B_i}. \tag{2}$$

The parallel potential is proportional to W_i so a larger potential is necessary to accelerate higher energy electrons. Is the following explanation satisfactory? AC6 dos1 electron energy response increases rapidly from 30 keV to a peak at 100 keV (O'Brien et al., 2019, Figure 2), therefore our assumption that $W_i = 30$ keV will underestimate the parallel potential. In reality, the counts observed by AC6 is a convolution of, among other things, the AC6 dos1 electron energy response and the falling electron energy spectrum. Thus, the majority of electrons that AC6 observed have energies close to 30 keV and the $W_i = 30$ is an appropriate approximation.

We again use IRBEM-Lib to estimate $q\Phi$. For each example curtain in Fig. 5, we first estimated the local magnetic field, B_f, that the electron descended to after the acceleration. Then we traced the local field line into the SAA. We found B_i at 100 kilometers altitude in the SAA for barely trapped electrons. With the initial and final B, along with $W = 30$ keV, the minimum potential must be $q\Phi = 1 - 4$ kV for the 4 examples shown in Fig. 5.

The range of estimated potentials is typical for the aurora. Partamies et al. (2008) used the observations made by the Fast Auroral SnapshoT (FAST) mission and reported that the auroral inverted-V electron precipitation structures, with electron energies up to a few tens of keV, were accelerated by 2-4 kV parallel potentials. The inverted-V structure and curtains share a number of similarities including: their extent in energy, latitudinal width, and high occurance rate in the midnight MLT region. One notable difference is the aurora is observed at higher L shells. A possible connection between the inverted-V structures is intriguing, but by itself AC6 can not easily test this hypothesis. A follow-on study can incorporate the list of observed curtains with ground-based auroral imagers and look for simultaneous occurrence of curtains and meso-scale auroral arcs.

Outside of the BLC, the lack of pitch angle information makes the AC6 electron data ambiguous, but the curtains observed in the BLC suggest that some curtains continuously precipitate for multiple seconds. Curtains could be a significant source of energetic electrons into the atmosphere. Energetic electron precipitation produces odd Nitrogen (HO_X) that is currently underestimated by atmospheric models such as the widely-used Whole Atmosphere Community Climate Model using Specified Dynamics (SD-WACCM) (e.g. Randall et al., 2015). A comprehensive study of the curtain impact on the atmosphere can be done with an AC6-like mission with pitch angle and energy resolution.

7 Conclusions

The 1634 confirmed curtains allowed us to make the following inferences:

1. Curtains are very narrow—90% are less than 21 kilometers wide in latitude.
2. Curtains are observed in the outer radiation belt, predominately in the midnight and the late morning MLT regions, during active geomagnetic periods.
3. At least some curtains continuously precipitate into the atmosphere for multiple seconds.

Curtains are remarkably narrow with fine structure that persist for multiple seconds. Either the scattering mechanism that continuously generates curtains is physically static for multiple seconds, or the curtain electron drift is often undisturbed.

The curtain-microburst relationship hypothesized in Blake and O'Brien (2016) is not clear. The two results in support of the hypothesis are: curtain width and microburst size distributions are very similar, and the limited AC6 sampling in MLT shows that both occur in similar locations in the magnetosphere. But curtains observed in the bounce loss cone complicate this interpretation. Some curtains continuously precipitate for at least a few seconds and can be a significant source of energetic electron precipitation into the atmosphere. Furthermore, we found that the continuous scattering of curtain electrons can be explained by a parallel direct current electric field so curtains may be related to the aurora.

Appendix A Distribution of Colocated 10 Hz Data

Figure A1 shows the distribution of colocated AC6 10 Hz data as a function of in-track lag. This distribution is weighted to small in-track lags and 72% of the colocated 10 Hz data was taken when AC6 were separated in-track by less than 10 seconds, corresponding to 75 km in-track separation. Therefore, most of the curtains studied here were observed for small in-track lags.

Acknowledgments

This work was made possible with the help from the many engineers and scientists at The Aerospace Corporation who designed, built, and operated AC6. M. Shumko was supported by NASA Headquarters under the NASA Earth and Space Science Fellowship Program - Grant 80NSSC18K1204 and NASA Postdoctoral Program at the NASA's Goddard Space Flight Center, administered by Universities Space Research Association under contract with NASA. D.L. Turner is thankful for support from the Van Allen Probes mission and a NASA grant (Prime award number: 80NSSC19K0280). The work at The Aerospace Corporation was supported in part by RBSP-ECT funding provided by JHU/APL contract 967399 under NASA's Prime contract NAS501072. The AC6 data is available at http://rbspgway.jhuapl.edu/ac6 and the IRBEM-Lib version used for this analysis can be downloaded from https://sourceforge.net/p/irbem/code/616/tree/.

References

Anderson, K. A., & Milton, D. W. (1964). Balloon observations of X rays in the auroral zone: 3. High time resolution studies. *Journal of Geophysical Research*, *69*(21), 4457–4479. Retrieved from `http://dx.doi.org/10.1029/JZ069i021p04457` doi: 10.1029/JZ069i021p04457

Blake, J. B., & O'Brien, T. P. (2016). Observations of small-scale latitudinal structure in energetic electron precipitation. *Journal of Geophysical Research: Space Physics*, *121*(4), 3031–3035. Retrieved from `http://dx.doi.org/10.1002/`

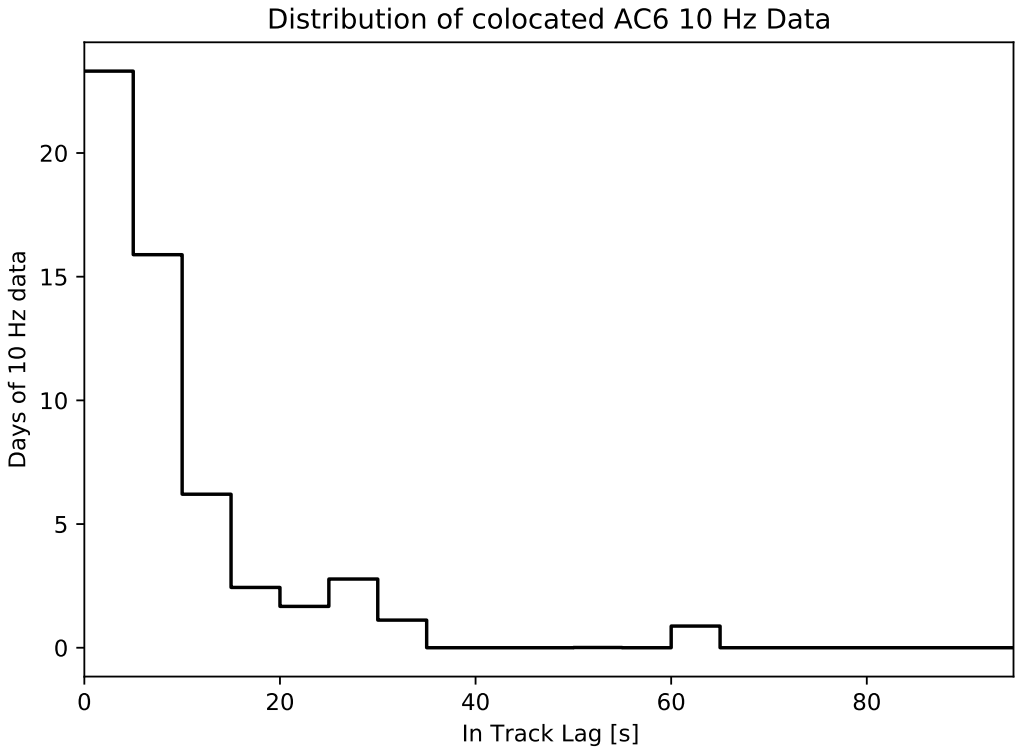

Figure A1. The distribution of colocated 10 Hz data as a function of in-track lag. Bins are 5 kilometers wide.

2015JA021815 (2015JA021815) doi: 10.1002/2015JA021815

Blum, L., Li, X., & Denton, M. (2015). Rapid MeV electron precipitation as observed by SAMPEX/HILT during high-speed stream-driven storms. *Journal of Geophysical Research: Space Physics*, *120*(5), 3783–3794. Retrieved from http://dx.doi.org/10.1002/2014JA020633 (2014JA020633) doi: 10.1002/2014JA020633

Boscher, D., Bourdarie, S., O'Brien, P., Guild, T., & Shumko, M. (2012). *Irbem-lib library.*

Breneman, A., Crew, A., Sample, J., Klumpar, D., Johnson, A., Agapitov, O., ... others (2017). Observations directly linking relativistic electron microbursts to whistler mode chorus: Van allen probes and FIREBIRD II. *Geophysical Research Letters*.

Brown, R., Barcus, J., & Parsons, N. (1965, 6). Balloon observations of auroral zone x rays in conjugate regions. 2. microbursts and pulsations. *Journal of Geophysical Research (U.S.)*, *70*. doi: 10.1029/JZ070i011p02599

Comess, M., Smith, D., Selesnick, R., Millan, R., & Sample, J. (2013). Duskside relativistic electron precipitation as measured by sampex: A statistical survey. *Journal of Geophysical Research: Space Physics*, *118*(8), 5050-5058. Retrieved from https://agupubs.onlinelibrary.wiley.com/doi/abs/10.1002/jgra.50481 doi: 10.1002/jgra.50481

Dietrich, S., Rodger, C. J., Clilverd, M. A., Bortnik, J., & Raita, T. (2010). Relativistic microburst storm characteristics: Combined satellite and ground-based observations. *Journal of Geophysical Research: Space Physics*, *115*(A12).

Douma, E., Rodger, C., Blum, L., O'Brien, T., Clilverd, M., & Blake, J. (2019). Characteristics of relativistic microburst intensity from sampex observations. *Journal of Geophysical Research: Space Physics*.

Douma, E., Rodger, C. J., Blum, L. W., & Clilverd, M. A. (2017). Occurrence characteristics of relativistic electron microbursts from SAMPEX observations. *Journal of Geophysical Research: Space Physics*, *122*(8), 8096–8107. Retrieved from http://dx.doi.org/10.1002/2017JA024067 (2017JA024067) doi: 10.1002/2017JA024067

Greeley, A., Kanekal, S., Baker, D., Klecker, B., & Schiller, Q. (2019). Quantifying the contribution of microbursts to global electron loss in the radiation belts. *Journal of Geophysical Research: Space Physics*.

Johnson, A., Shumko, M., Griffith, B., Klumpar, D., Sample, J., Springer, L., ... others (2020). The firebird-ii cubesat mission: Focused investigations of relativistic electron burst intensity, range, and dynamics. *Review of Scientific Instruments*, *91*(3), 034503.

Lehtinen, N. G., Inan, U. S., & Bell, T. F. (2000). Trapped energetic electron curtains produced by thunderstorm driven relativistic runaway electrons. *Geophysical research letters*, *27*(8), 1095–1098.

Lorentzen, K. R., Blake, J. B., Inan, U. S., & Bortnik, J. (2001). Observations of relativistic electron microbursts in association with VLF chorus. *Journal of Geophysical Research: Space Physics*, *106*(A4), 6017–6027. Retrieved from http://dx.doi.org/10.1029/2000JA003018 doi: 10.1029/2000JA003018

Lorentzen, K. R., Looper, M. D., & Blake, J. B. (2001). Relativistic electron microbursts during the GEM storms. *Geophysical Research Letters*, *28*(13), 2573–2576. Retrieved from http://dx.doi.org/10.1029/2001GL012926 doi: 10.1029/2001GL012926

O'Brien, T. P., Blake, J. B., & W., G. J. (2016, May). *AeroCube-6 dosimeter data README* (Tech. Rep. No. TOR-2016-01155). The Aerospace Corporation.

O'Brien, T. P., Looper, M. D., & Blake, J. B. (2019, July). *AeroCube-6 dosimeter equivalent energy thresholds and flux conversion factors* (Tech. Rep. No. TOR-2017-02598). The Aerospace Corporation.

O'Brien, T. P., Lorentzen, K. R., Mann, I. R., Meredith, N. P., Blake, J. B., Fen-

nell, J. F., ... Anderson, R. R. (2003). Energization of relativistic electrons in the presence of ULF power and MeV microbursts: Evidence for dual ULF and VLF acceleration. *Journal of Geophysical Research: Space Physics*, *108*(A8). Retrieved from http://dx.doi.org/10.1029/2002JA009784 doi: 10.1029/2002JA009784

Olson, W. P., & Pfitzer, K. A. (1982). A dynamic model of the magnetospheric magnetic and electric fields for july 29, 1977. *Journal of Geophysical Research: Space Physics*, *87*(A8), 5943–5948. Retrieved from http://dx.doi.org/10.1029/JA087iA08p05943 doi: 10.1029/JA087iA08p05943

Parks, G. K. (1967). Spatial characteristics of auroral-zone X-ray microbursts. *Journal of Geophysical Research*, *72*(1), 215–226.

Partamies, N., Donovan, E., & Knudsen, D. (2008). Statistical study of inverted-v structures in fast data. In *Annales geophysicae* (Vol. 26, pp. 1439–1449).

Randall, C. E., Harvey, V. L., Holt, L. A., Marsh, D. R., Kinnison, D., Funke, B., & Bernath, P. F. (2015). Simulation of energetic particle precipitation effects during the 2003–2004 arctic winter. *Journal of Geophysical Research: Space Physics*, *120*(6), 5035–5048.

Seppälä, A., Douma, E., Rodger, C., Verronen, P., Clilverd, M. A., & Bortnik, J. (2018). Relativistic electron microburst events: Modeling the atmospheric impact. *Geophysical Research Letters*, *45*(2), 1141–1147.

Shumko, M., Johnson, A., Sample, J., Griffith, B. A., Turner, D. L., O'Brien, T. P., ... Claudepierre, S. G. (2019). Electron microburst size distribution derived with aerocube-6. *Journal of Geophysical Research: Space Physics*, e2019JA027651.

Thorne, R. M., O'Brien, T. P., Shprits, Y. Y., Summers, D., & Horne, R. B. (2005). Timescale for MeV electron microburst loss during geomagnetic storms. *Journal of Geophysical Research: Space Physics*, *110*(A9). Retrieved from http://dx.doi.org/10.1029/2004JA010882 (A09202) doi: 10.1029/2004JA010882

Tsyganenko, N. (1989). A solution of the chapman-ferraro problem for an ellipsoidal magnetopause. *Planetary and Space Science*, *37*(9), 1037 - 1046. Retrieved from http://www.sciencedirect.com/science/article/pii/0032063389900767 doi: http://dx.doi.org/10.1016/0032-0633(89)90076-7